Indian Journal of Pure & Applied Physics
Vol. 63, October 2025, pp. 952-960
DOI: 10.56042/ijpap.v63i10.20922

Metamaterial Based Frequency Reconfigurable Antenna for C/X-Band Applications

Amsaveni A*, Bharathi M, Tharun R B & Madhavan T
Department of Electronics and communicaton Engineering, Kumaraguru College of Technology, Coimbatore 641 049, India

Received: 24th June 2024; accepted: 25th August 2025

This paper presents the design and analysis of a high-gain, metamaterial-inspired antenna with frequency reconfigurability, targeting multiband operation across the C and X bands for modern wireless communication applications. The proposed antenna incorporates Complementary Split-Ring Resonators (CSRRs) within a rectangular patch to achieve frequency agility, enhanced impedance matching, and improved radiation performance. Simulated on a FR4epoxy substrate, the antenna is equipped with a PIN diode to enable dynamic switching between operational states. In the ON state, the antenna resonates at 4.84 GHz, 7.97 GHz, and 8.69 GHz, delivering peak gains of up to 6.83 dB with stable, directional radiation patterns in both E-plane and H-plane. In the OFF state, the resonant band shifts to 5.34–5.75 GHz, maintaining a moderate gain of 4.53 dB and consistent radiation behavior. Ansys HFSS simulation software is used to assess the antenna's performance, and important parameters like gain, radiation patterns, and S-parameters are carefully examined. Findings show that the antenna has acceptable gain characteristics, a broad bandwidth, and efficient frequency reconfigurability, making it a viable option for IoT and radar systems and Satellite communications.

Keywords: Metamaterial, Frequency reconfigurability, Complementary split-ring resonator, Defected ground structure, Multiband antenna

1 Introduction

Small, high-gain antennas with multiband functionality have always been in demand due to the rapid growth in wireless communication. These C (4-8 GHz) and X (8-12 GHz) bands are becoming increasingly popular with satellite communications, RADAR systems, and modern wireless networks of the likes of 5G and IoT. Traditional antenna designs are often not able to cope with these requirements as they tend to offer fixed operating frequencies, limited gain performance, and poor adaptability across multiple bands. This limits proper spectral usage and compromises transmission efficiency, putting signal integrity at stake in environments where more than one communication standard coexists.

Frequency reconfigurable antennas present themselves as one of the promising solutions to reduce hardware complexity, cost, and space needs of multipurpose devices by allowing the same antenna structure for operating at various frequencies. Innovative design mechanisms are demanded to realize frequency reconfigurability without compromising radiation performance or compactness.

Metamaterials significantly enhance antenna performance. They are artificially constructed formations having peculiar electromagnetic properties such as negative permittivity and permeability. Metamaterial-enabled enhanced gain, miniaturization, and frequency agility may be achieved through the placement of metamaterial unit cells such as split-ring resonators (SRRs) or complementary split-ring resonators (CSRRs). Hence, metamaterial-based reconfigurable antennas are attractive for C/X-band applications owing to the trade-off between size and performance[1].

A circular patch antenna integrated with split-ring resonators (SRRs) has been designed for satellite communications applications. The proposed configuration demonstrated multiband operations with enhanced gain, proving the effectiveness of metamaterials toward performance enhancement for space systems[2]. Likewise, a quarter-circular microstrip antenna embedded with metamaterials, operating at 3.5 GHz, is investigated. Their study emphasized compactness and efficiency, which are two foremost features of subwavelength-scale communication technologies[3-4].

To improve flexibility and communication efficiency in Internet of Things applications, a smart meta-surface based antenna with both pattern and beam reconfigurability has been developed[5]. Furthermore, frequency-selective surfaces have been investigated for

*corresponding author: E-mail: amsaveni.a.ece@kct.ac.in

beam-switching capabilities, which allow for dynamic coverage and enhanced adaptability in wireless systems[6–7].

More recently, frequency reconfigurable antennas that employ varactors, PIN diodes, and RF-MEMS switches have been proposed to operate dynamically. However, these solutions are often complex to integrate and require biasing circuitry. On the other hand, a metamaterials-based design achieves reconfigurability in a more passive and condensed way. In[8–10], a triband antenna with an SRR array was suggested; it produced ideal radiation patterns across multiple bands and an acceptable return loss.

Even with these advancements, it is still difficult to achieve compactness and reconfigurability simultaneously across wideband C/X-band operations. Many current works either require intricate switching mechanisms or are restricted to static multiband performance. For C/X-band operations, the present work suggests a compact frequency reconfigurable antenna structure that is packed with metamaterial components. The structure uses a combination of metamaterial integration and geometrical reconfiguration to achieve frequency tuning.

2 Antenna Design Methodology

The proposed antenna is a frequency reconfigurable rectangular patch antenna designed for operation across the C, and X bands. The structure integrates a PIN diode and metamaterial-inspired elements to enable dynamic switching of resonant frequencies. The design focuses on optimizing radiation performance in both ON and OFF diode states while maintaining compactness and efficient impedance matching.

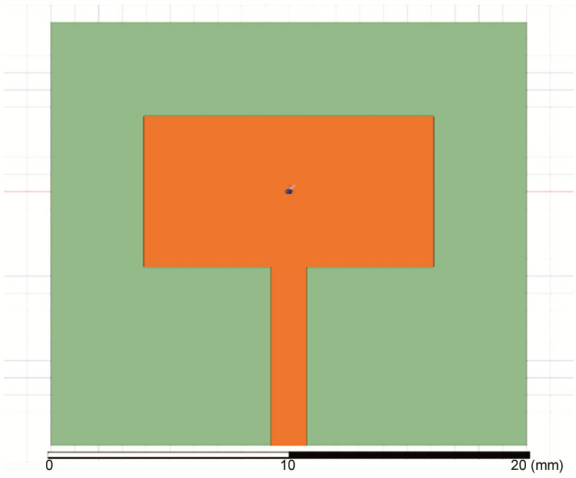

Fig. 1 — Rectangular patch antenna

2.1 Conventional Rectangular Patch Antenna

The design process begins with the development of a basic rectangular microstrip patch antenna, measuring 14.7 mm × 19.4 mm, intended to operate at a center frequency of 4.8 GHz, as illustrated in Fig. 1. The antenna is simulated on an FR4 epoxy substrate characterized by a relative permittivity of 4.2 and a thickness of 1.6 mm. Fundamental parameters—including patch dimensions, effective dielectric constant (ε_{eff}), and other critical design values—are determined using conventional transmission line model equations. The calculated parameters are summarized in Table 1.

The width of the microstrip patch, W_P, is determined using the equation:

$$W_P = \frac{c}{2fr}\sqrt{\frac{2}{\varepsilon_r+1}} \quad \ldots (1)$$

The patch length, L_P, is calculated by subtracting the fringing field extension (2ΔL) from the effective length Leff:

$$L_P = L_{eff} - 2\Delta L \quad \ldots (2)$$

The effective length L_{eff} is given by,

$$L_{eff} = \frac{c}{2f\sqrt{\varepsilon_{reff}}} \quad \ldots (3)$$

where f_r = Resonant frequency, ε_{reff}= Effective Dielectric constant, c = Velocity of wave

The extension of the length due to fringing fields (ΔL) is calculated as:

$$\Delta L = 0.412\frac{(\varepsilon+0.3)\left(\frac{W}{h}-0.264\right)}{(\varepsilon-0.258)\left(\frac{W}{h}-0.8\right)} \quad \ldots (4)$$

The effective dielectric constant ε_{reff} is estimated by:

$$\varepsilon_{reff} = \frac{\varepsilon+1}{2} + \frac{\varepsilon-1}{2}\left[1+12\frac{h}{W}\right]^{-\frac{1}{2}} \quad \ldots (5)$$

Table 1 — Dimensions of the Antenna

Parameters	Values
Patch Width, PW	19.4 mm
Patch Length, PL	14.7 mm
Substrate Width, SW	29.0 mm
Substrate Length, SL	24.3 mm
S1,S3	2.0 mm
S2,S4	1.0 mm
G1,G4	4.8 mm
G2	3.0 mm
G3	0.5 mm

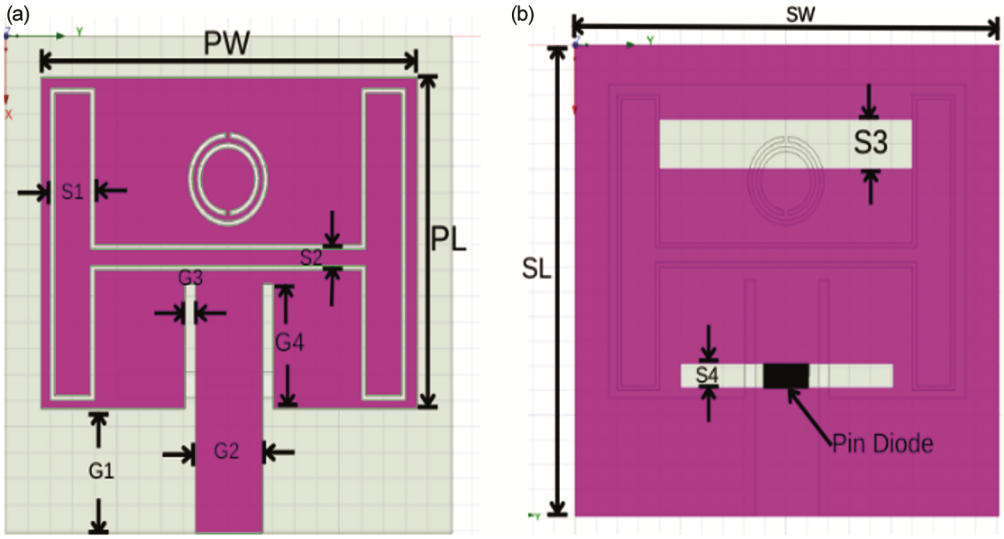

Fig. 2 — Antenna Structure (a) front view (b) back View

The dimensions of the substrate are defined as:

$$L_s = L + 6h \quad \ldots (6)$$

$$W_s = W + 6h \quad \ldots (7)$$

The antenna dimensions, including patch size, slot positions, and CSRR geometry, were selected through iterative parametric analysis to optimize resonance at target C/X band frequencies. These parameters ensured proper impedance matching, gain enhancement, and compactness.

2.2 Reconfigurable Patch Antenna with CSRR and Slots

The proposed antenna (Fig. 2) includes a rectangular radiating patch loaded with a Complementary Split-Ring Resonator and multiple narrow slots (S1, S2) on either side to enable multi-resonant behaviour and to enhance surface current path. The slots are carefully positioned and dimensioned through parametric analysis to excite multiple resonant modes. The gaps G1–G4 controls the spacing and impedance characteristics between patch segments.

The ground plane (shown in Fig. 2b) is slotted to accommodate a PIN diode that enables switching between frequency states. The slots S3 and S4 are introduced to support reconfigurability and adjust the effective current path in each state. The slot S3 affects the magnetic field interaction with the patch, critical for gain improvement in reconfigured modes. The narrow slot near the diode, S4, is tuned to influence isolation and improve impedance matching in the OFF state.

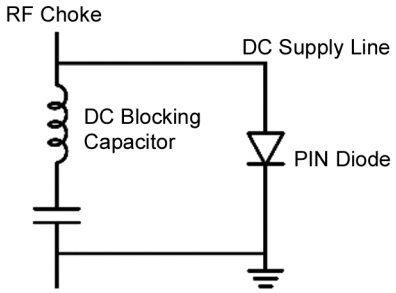

Fig. 3 — Biasing network for PIN diode

A PIN diode is embedded in the slot gap between the CSRR and the feed network to achieve frequency reconfigurability. As shown in Fig. 3, this switching mechanism is realized using an isolated DC biasing network consisting of RF chokes and DC blocks, ensuring negligible impact on the RF characteristics.

A Complementary Split Ring Resonator (CSRR) structure shown in Fig. 2 consists of two concentric metallic rings etched on the ground plane or metal surface, with gaps and a narrow-split section. The CSRR acts as a left-handed metamaterial unit, contributing to both miniaturization and resonance shaping. The CSRR design parameters are optimized to achieve double-negative effective permittivity and permeability in the desired frequency range.

These physical dimensions influence the resonant frequency by altering the effective inductance and capacitance of the resonator.The CSRR behaves as an LC resonator, and its equivalent circuit includes series inductors L, a shunt capacitance C between the line and ground and a parallel LC tank circuit as shown in Fig.4.

The resonant frequency of the CSRR is determined by the LC components and is given by:

$$f_r = \frac{1}{2\pi\sqrt{L_C C_C}} \quad \ldots (8)$$

where:

i fr : Resonant frequency (Hz)
ii L_C : Inductance due to loop current (depends on ring size and trace width)
iii C_C : Capacitance between the rings and across gaps

The capacitance between the rings can be approximated by:

$$C_C \approx 2\pi\varepsilon_O \frac{rh}{g} \quad \ldots (9)$$

where:

i ε_0 : Free space permittivity (~8.854×10^{-12} F/m)
ii ε_r : Substrate relative permittivity
iii r : Average radius of the rings
iv h: Substrate height or thickness of the conductive layer
v g: Gap between the rings

Inductance of the resonator can be estimated using,

$$L_C \approx \mu_o r \left[\ln\left(\frac{8r}{c}\right) - 2\right] \quad \ldots (10)$$

where:

i μ_0 : Free space permeability (~$4\pi \times 10^{-7}$ H/m)
ii r: Average radius
iii c: Conductor width

Figure 5 illustrates the equivalent circuit representations of a PIN diode in its two primary operating states—forward-biased (ON state) and reverse-biased (OFF state.

In the ON state (Forward Biased), the PIN diode conducts, acting nearly as a short circuit with minimal impedance. The equivalent circuit is modelled using a series combination of a small resistance Rs=1.4 Ω and an inductance Ls=0.6 nH. The series resistance represents the conduction losses, while the inductance models the parasitic effect due to packaging and the diode's internal structure. This configuration allows RF current to pass through, effectively connecting or activating specific sections of the antenna.

In the OFF state (Reverse Biased), the diode behaves as an open circuit, and its equivalent model consists of the same parasitic inductance Ls=0.6 nH in series with a parallel RC branch, where Rp=10 kΩ (representing high isolation) and Cp=0.5 pF (parasitic capacitance). The high resistance ensures minimal current flow, effectively isolating sections of the circuit, while the small capacitance may allow limited high-frequency leakage.

The backside of the antenna incorporates a Defected Ground Structure (DGS) in the form of two narrow rectangular slots (S3 and S4). The DGS introduces an additional degree of freedom in controlling current distribution and suppressing surface waves. The DGS is co-designed with the CSRR to synergize resonance performance and minimize back radiation losses.

Table 2 presents the calculated electromagnetic characteristics - namely, the effective permittivity

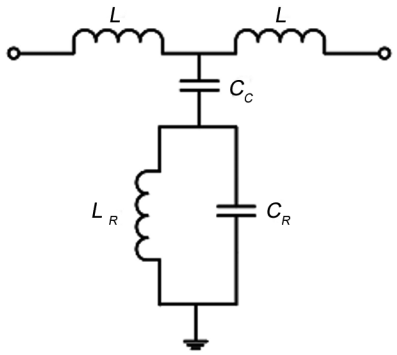

Fig. 4 — CSRR Equivalent circuit

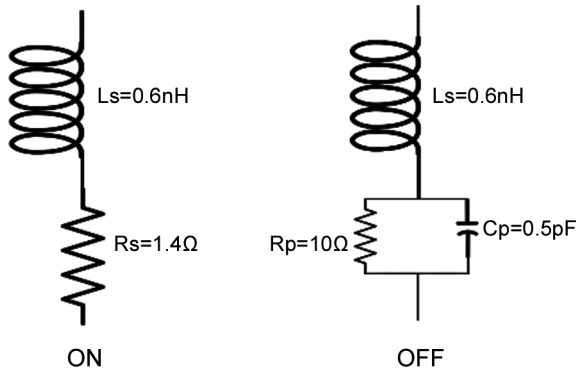

Fig. 5 — PIN Diode Equivalent Circuit Model

Table 2 — Electromagnetic Parameters at Different Frequencies

Frequency (GHz)	Permittivity (εeff)	Permeability (μeff)	Interpretation
4.84	–1.7	–0.9	Negative index (S-band)
7.97	–2.4	–1.3	Strong lefthanded region (X-band)
8.69	–1.2	–1.1	Negative refractive index
5.34–5.75 (OFF)	~0.4	~0.6	No negative behavior

($\varepsilon_e$ff) and permeability ($\mu_e$ff)-of the proposed metamaterial-inspired antenna at various resonant frequencies. The results show that the antenna acts like a metamaterial when it is in the ON-state, displaying negative values of $\varepsilon_e$ff and $\mu_e$ff at certain frequencies. In contrast, the OFF-state emphasizes the antenna's capability to switch between different electromagnetic responses by reflecting standard dielectric properties with positive parameter values. These values are essential for understanding and evaluating the material performance and resonance mechanisms of the antenna under different operating conditions.

3 Results and Discussion

The antenna was simulated in Ansys HFSS using radiation boundaries to simulate free-space conditions. A wave port was used for excitation, and adaptive meshing was applied with local refinement near critical features to ensure accurate S-parameter results.The simulated results are analyzed to assess the antenna's performance across key parameters, including return loss (S_{11}), gain, radiation characteristics, and electric field distribution. The analysis considers the two switching conditions of the PIN diode—forward-biased (ON) and reverse-biased (OFF)—to demonstrate the antenna's capability to transition between multiband and single-band modes. Additionally, the influence of the integrated Complementary Split Ring Resonator (CSRR) and Defected Ground Structure (DGS) on resonant frequency tuning, impedance matching, and radiation efficiency is investigated to confirm the antenna's suitability for C, and X band wireless applications.

3.1 Performance in Diode ON State

When the PIN diode is forward biased (ON), the antenna exhibits multiband behaviour, as illustrated in Fig. 6. The reflection coefficient (S_{11}) shows deep nulls at 4.84 GHz, 7.97 GHz, and 8.69 GHz, each falling below the −10 dB threshold, indicating effective impedance matching and strong resonance. As shown in Fig. 7, the realized gain increases with frequency, achieving values of 3.68 dB at 4.84 GHz, 4.48 dB at 7.97 GHz, and a peak of 6.83 dB at 8.69 GHz. This confirms the antenna's suitability for frequency-agile wireless applications.

The radiation patterns for the E-plane and H-plane in this configuration, depicted in Figs. 8-9 respectively, exhibit well-defined directional characteristics. At 4.84 GHz, the E-plane pattern is broad and quasi-omnidirectional, while the H-plane displays a figure-eight configuration. At higher frequencies, such as 7.97 GHz and 8.69 GHz, both planes show narrower, more focused beams, reflecting enhanced directivity and reduced side lobes—features desirable in radar and high-frequency communication systems.

The corresponding electric field distributions are presented in Fig. 10. The front view (Fig. 10a) shows strong field localization near the slot edges, CSRR, and transmission line, indicating efficient energy confinement and enhanced radiation performance due

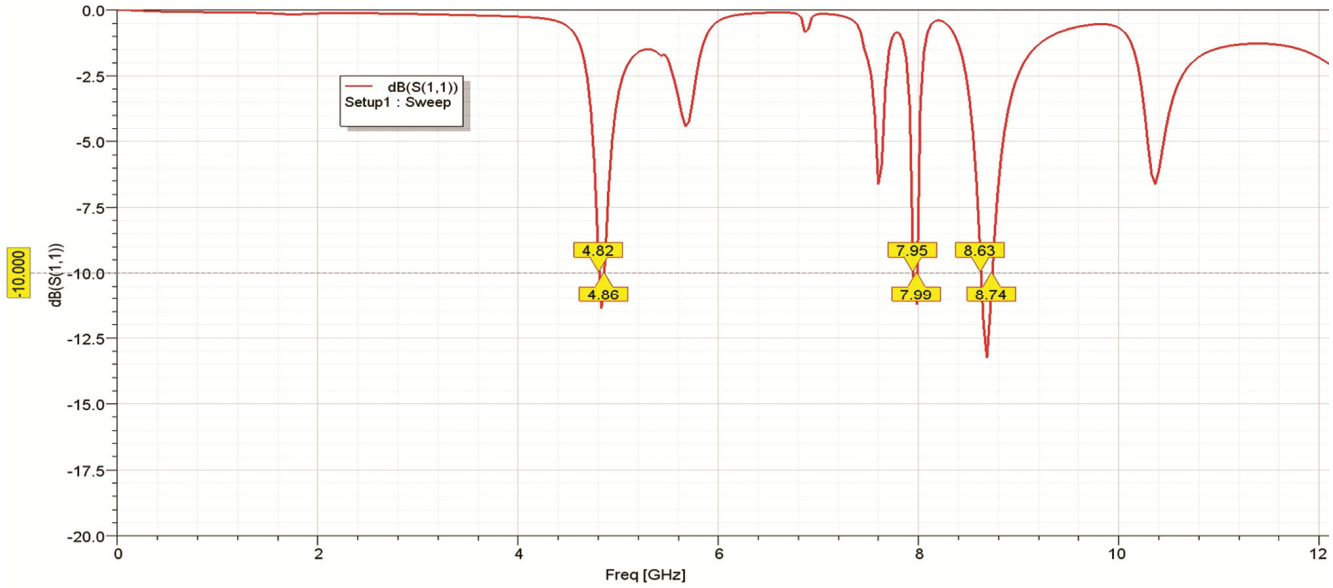

Fig. 6 — Simulated Reflection Co-efficient $S_{11}$of the proposed antenna during ON State

to the activated resonating elements. The back view (Fig. 10b) reveals a wide field spread around the feed and ground slots, with peak intensity reaching 128.442 KV/m. The performance measures during ON state are summarized in Table 3.

3.2 Performance in Diode OFF State

In the reverse biased (OFF) condition, the antenna transitions to a single-band operation. As shown in Fig. 11 the S_{11} curve (red curve) exhibits a resonant dip at 5.62 GHz, confirming narrowband behavior.

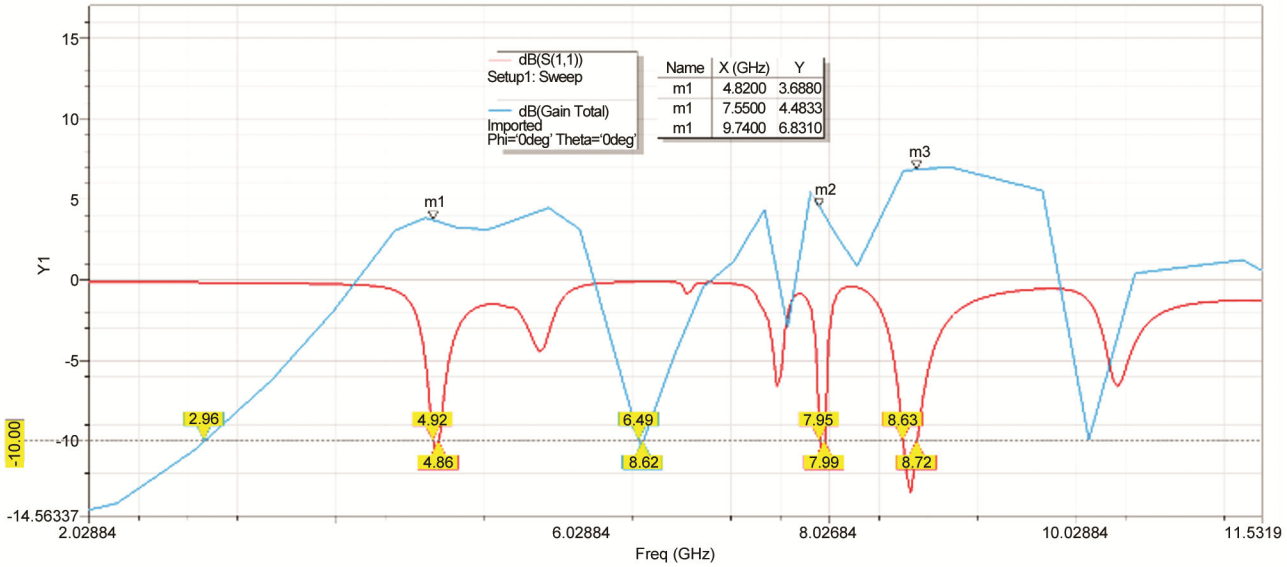

Fig. 7 — Simulated S_{11} and Gain during ON State

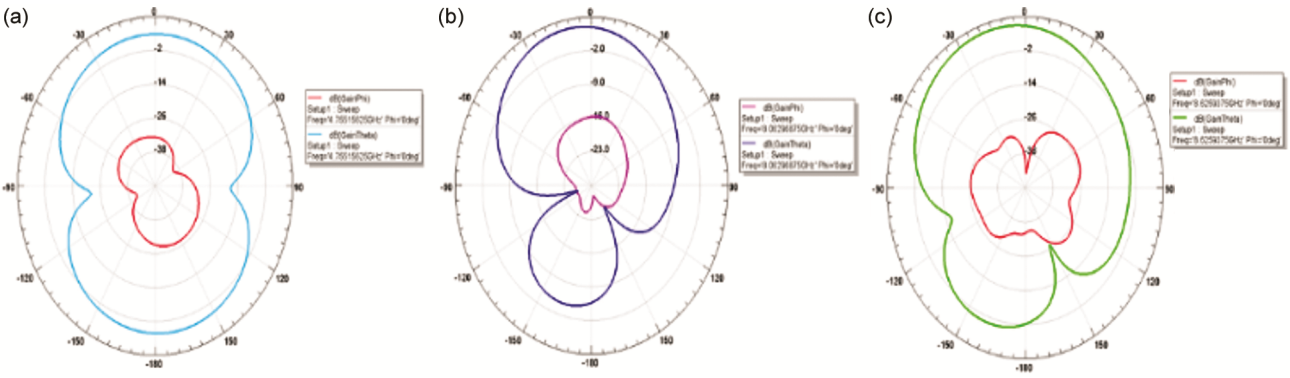

Fig. 8 — E-Plane in ON State

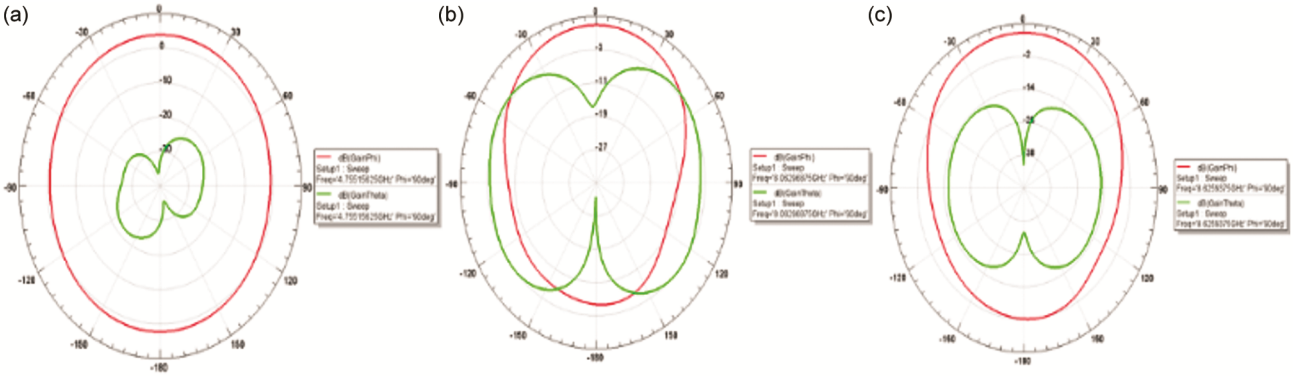

Fig. 9 — H-Plane in ON State

The gain(blue curve) peaks at 4.53 dB, slightly lower than in the ON state, yet sufficient for practical use in satellite and radar systems.

The radiation characteristics at this state are illustrated in Fig. 12. The E-plane at 5.63 GHz demonstrates a clearly defined main lobe with minimal cross-polarization, ensuring stable vertical radiation. Meanwhile, the H-plane exhibits a wide figure-eight pattern, consistent with horizontal directivity suitable for point-to-point communication links.

The Electric field distributions during the OFF state, shown in Fig. 13, reveal a concentrated field near the feed and resonating sections. The peak field intensity reaches 47,732.863 V/m, lower than the ON state, indicating reduced radiation efficiency. However, the consistent field pattern confirms that the

Table 3 — Performance of the proposed antenna during ON State

Parameter	Specification
Resonant Frequency (GHz)	4.84, 7.97, 8.69
Operating Bands(GHz)	4.82-4.86,7.95-7.99, 8.63-8.74
Bandwidth (GHz)	0.04/0.04/0.11
Return Loss (dB)	-11.5/-11.3/-13.3
Gain (dB)	3.68, 4.48, 6.83
Applications	Wi-Fi, Bluetooth, ISM, Radar, Satellite

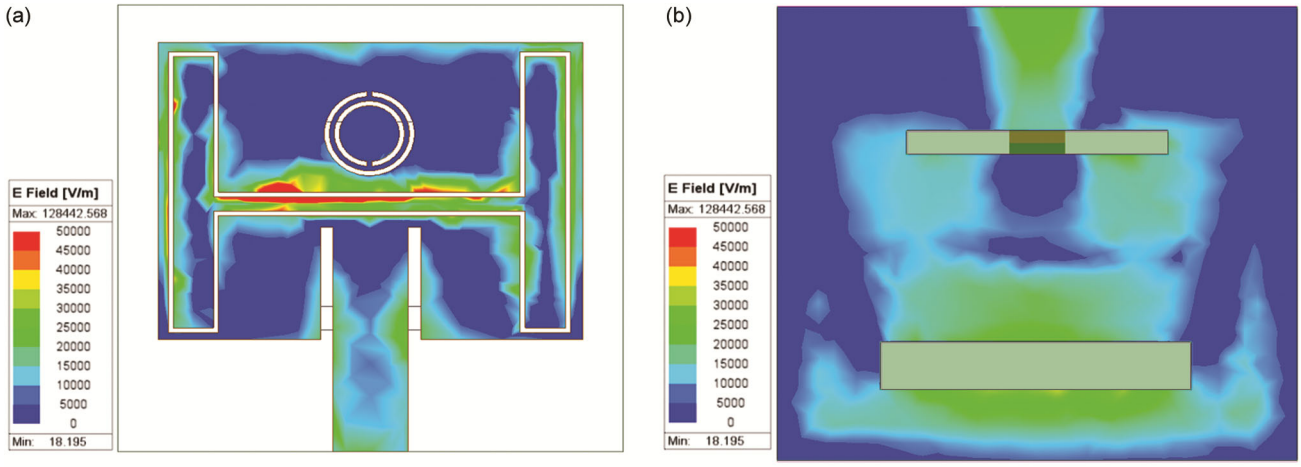

Fig. 10 — Electric Field Distribution a) Front View (b) Back View

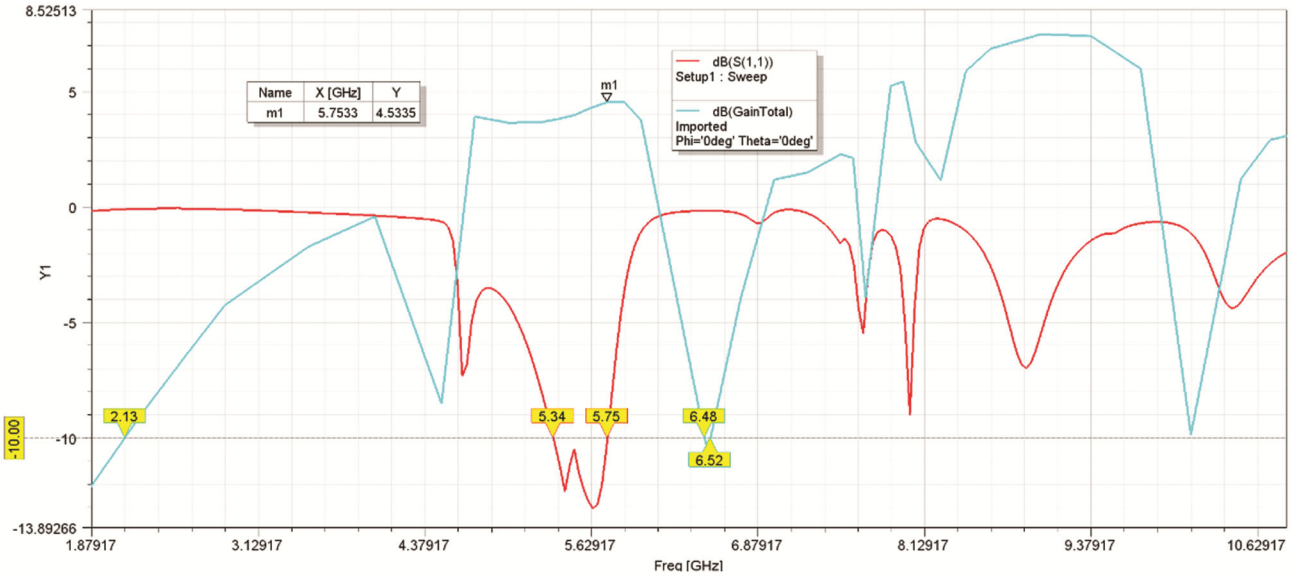

Fig. 11 — Simulated Reflection Co-efficient S_{11} and Gain of the proposed antenna during OFF State

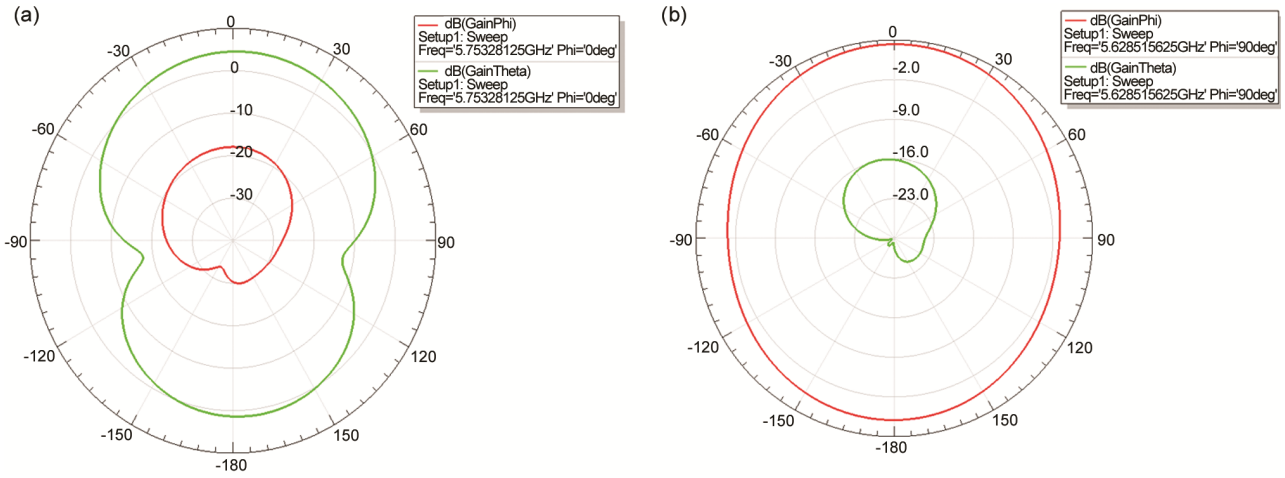

Fig. 12 — Simlated Radiation Pattern during PIN diode OFF state at 5.62 GHz (a) E-Plane (b) H-Plane

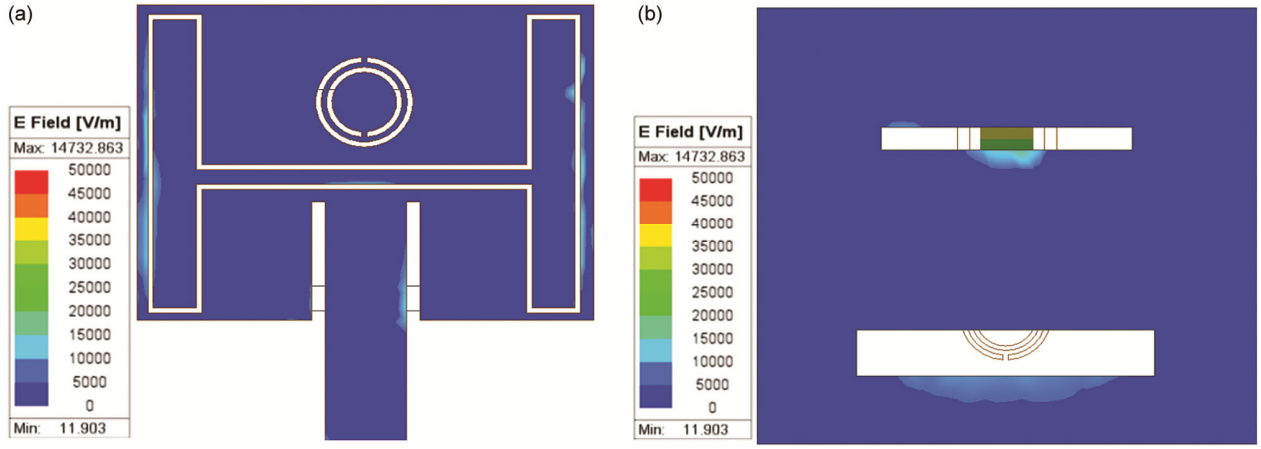

Fig. 13 — E-Field Distribution (a) Front View (b) Back View

Table 4 — Performance Comparison Between ON and OFF States

Parameter	Diode ON State	Diode OFF State
Resonant Frequencies (GHz)	4.84, 7.97, 8.69	5.62
Operating Band	Multiband	Single Band
Peak Gain (dB)	6.83	4.53
Radiation Pattern	Directional with sharp beams	Broad with stable lobes
Electric Field Intensity	1.28 MV/m	47.73 KV/m
Applications	Wi-Fi, ISM, Zigbee, RFID, 5G	Satellite, Radar Systems

structure maintains acceptable performance with reliable impedance matching and radiation stability.

Table 4 presents a comparative summary of the antenna's performance in both ON and OFF diode states. The ON-state supports multiple resonant modes with higher peak gain and improved directivity, while the OFF-state is optimized for single-band operation with stable radiation characteristics.

3.3 Comparison with Existing Works

Table 5 presents a comparative analysis of the proposed antenna design against selected existing works reported in the literature. The present work demonstrates multiband operation at centre frequencies of 4.84 GHz, 7.97 GHz, and 8.69 GHz, whereas the reference designs operate at single or fewer bands. The gain performance of the proposed design ranges from 3.68 dBi to 6.83 dBi, indicating efficient radiation, especially at higher bands. This is on par with or better than the gain values reported in [2,12], and closely matches the performance of[11]. The return loss values (S_{11}) fall between –11.30 dB and –13.30 dB, suggesting excellent impedance matching across all resonant frequencies.

Table 5 — Performance Comparison of the Proposed Antenna with Existing Work

Performance Measure	Kaur *et al*.[11] (2021)	Roy & Chakraborty[12] (2022)	Anitha *et al*.[2] (2024)	Proposed Work
Operating Band (GHz)	1.30 -12.73 14.83–20.00	1.60 - 2.80 5.10– 60.00	Multiple Bands	4.82-4.86, 7.95-7.99, 8.63-8.74
Bandwidth (GHz)	11.43/5.17	1.20 / 0.90	<0.05	0.04 / 0.04 / 0.11
Gain (dBi)	3.9 – 5.2	1.50 – 2.500	4.50	3.68 – 6.83
Return Loss (S_{11} in dB)	–18.50 to –26.10	–20.40 to –28.30	–18.00	–11.30 to –13.30
Antenna Type	Fractal Patch + SRR + Rectangular Stubs	Planar Patch+ Frequency Reconfigurable Element	Circular Patch + SRR Metamaterial	Rectangular Patch + CSRR + DGS +
Reconfigurability	No	Yes	No	Yes
Application	WLAN, WiMAX, Bluetooth	Wearable ISM/WLAN Applications	Wi-fi	Wi-Fi, WLAN, Radar, Satellite Communication

Our design achieves simultaneous multiband operation with dynamic switching using a minimal component count. Unlike[2,11,12], our antenna incorporates a synergistic combination of CSRR and DGS with strategically placed slots and optimized PIN diode placement, resulting in compact size, better directivity, and improved gain in the X-band Structurally, the proposed antenna employs a combination of Complementary Split Ring Resonator (CSRR) and Defected Ground Structure (DGS), while the other designs utilize conventional patch structures with or without SRR loading. Notably, the proposed design and[2] support frequency reconfigurability, a key feature lacking in[1,3].

4 Conclusion

A metamaterial-based frequency reconfigurable microstrip antenna has been designed and evaluated for efficient operation across C, and X bands. The antenna integrates a PIN diode to facilitate dynamic switching between multiband and single-band modes. In the ON state, the antenna exhibits resonant frequencies at 4.84 GHz, 7.97 GHz, and 8.69 GHz, with corresponding peak gains of 3.68 dB, 4.48 dB, and 6.83 dB, respectively. The return loss (S_{11}) at each of these frequencies falls well below −10 dB, indicating effective impedance matching and low reflection.In the OFF state, the antenna operates within a single band, resonating between 5.34 GHz and 5.75 GHz, and achieves a peak gain of 4.53 dB, maintaining acceptable performance with moderate bandwidth. Radiation pattern analysis confirms that the antenna maintains directional characteristics across all operating frequencies, with sharper and more focused beams observed at higher frequencies. The incorporation of CSRR and DGScontributes significantly to performance enhancement, offering improved current confinement, miniaturization, and enhanced radiation efficiency. As future work, the design will be fabricated and tested to verify simulated results, and advanced switching techniques such as MEMS or Varactor diode-based tuning will be explored for improved performance in real-world applications.

References

1 Tariq S, Rahim A A, Sethi W T, Faisal F & Djerafi T, *AEU Int J Electron Comm*, 177 (2024) 155195.

2 Anitha V R, Palanisamy S, Khalaf O I, Algburi S & Hamam H, *ICT Express*, 10 (4) (2024) 836.

3 Amsaveni A &Anusha K, *Int J Pure Appl Math*, 116 (11) (2017) 81.

4 Lu H, Xu X & Wei H, *Appl Comp Electromagn Soc J (ACES)*, 39 (2024) 327.

5 Awan W A, Hussai N, Park S G & Kim N, *Alexandria Eng J*, 92 (2024) 50.

6 Bouslama M, Traii M, Denidni T A & Gharsallah A, *IET Microw Antennas Propag*, 11 (1) (2017) 69.

7 Amsaveni A, BharathiM & Swaminathan J N, *Microsyst Technol*, 25 (6) (2019) 2273.

8 Painam S & Bhuma C, *IEEE Antennas Propag Magazine*, 61 (1) (2019) 91.

9 Rajeshkumar V & Rajkumar R, *Prog Electromagn Res Lett*, 95(2021) 43.

10 Tran H H, Bui C D, Nguyen-Trong N & Nguyen T K, *IEEE Access*, 9 (2021) 42325.

11 Kaur N, Sivia J S & Kumar M, *Wireless Personal Comm*, 120 (1) (2021) 515.

12 Roy S & Chakraborty U, *Wireless Personal Comm*, 127 (4) (2022) 3659.